

Optimal Design of an Alignment-Free Two-DOF Rehabilitation Robot for the Shoulder Complex

Daniel Galinski, Julien Sapin and Bruno Dehez, *Member, IEEE*

Abstract—This paper presents the optimal design of an alignment-free exoskeleton for the rehabilitation of the shoulder complex. This robot structure is constituted of two actuated joints and is linked to the arm through passive degrees of freedom (DOFs) to drive the flexion-extension and abduction-adduction movements of the upper arm. The optimal design of this structure is performed through two steps. The first step is a multi-objective optimization process aiming to find the best parameters characterizing the robot and its position relative to the patient. The second step is a comparison process aiming to select the best solution from the optimization results on the basis of several criteria related to practical considerations. The optimal design process leads to a solution outperforming an existing solution on aspects as kinematics or ergonomics while being more simple.

Index Terms—Exoskeleton, robot, design, rehabilitation, shoulder, alignment-free, self-aligning, optimization, genetic algorithm.

I. INTRODUCTION

STROKE that results in partial or complete hemiparesis is the main cause of disability [1], and this condition is worsening mainly due to ageing of the population [2]. For stroke patients, the goal of rehabilitation is to regain the highest level of motor function in order to recover the highest autonomy in daily living activities. This is even better achieved when the intensity of rehabilitation is high both in terms of duration and frequency [3].

In this context, the use of robotic devices seems well suited because such devices are able to perform repetitive and functional movements with high repeatability and they are less tiresome for the therapist than classical therapy [3]–[5]. Moreover, robotic devices can perform quantitative and objective measurements [6] and assist the patient through innovative control strategies.

The upper-limb rehabilitation robots can be classified into two categories according to their connection to the patient and their kinematics structure. On one hand, end-effector robots are connected to a distal part of the upper-limb and try to move the whole arm through this link. On the other hand, exoskeletons are linked to each segment of the upper-limb and try to drive all degrees-of-freedom (DOFs) independently of the others. In the present study, we focus exclusively on exoskeletons for the shoulder complex rehabilitation. In classical exoskeleton designs, the upper-limb is considered as

a succession of mechanical joints and the exoskeleton tries to reproduce the same kinematics chain by aligning the robot joints on the patient's joints.

There are mainly two problems with a such strategy. Firstly, the patient's joints can rarely be considered as simple mechanical joints, especially regarding their whole amplitude of motion. Secondly, the robot must be exactly matched to every patient due to the inter- and intra-subject bio-mechanical parameters variability. These drawbacks involve usually misalignment problems which may cause pain or harm the patient.

In response to this challenge, numerous exoskeletons have additional DOFs in their proximal kinematics chain to align at best the actuated robot joints with those of the patient. In these so-called self-aligning exoskeletons, the additional DOFs are free or are actuated and controlled through a zero force control-loop. Armin III [7] has one actuated linear DOF for the compensation of the scapular elevation-depression (SED) while the Pneu-WREX [8] has one actuated rotational DOF for the compensation of the scapular protraction-retraction (SPR). The design developed by Stienen et al. [9] presents two passive linear DOFs to compensate both SED and SPR. The IntelliArm [10] design has one actuated linear DOF for the compensation of the SED and two additional passive linear DOFs to match as best the robot joints to the patient's joints. On the other hand, the exoskeleton developed by Koo et al. [11] integrates two actuated rotational DOFs and one actuated linear DOF for the compensation of the SPR and the SED respectively. In addition to these actuated DOFs, one passive linear joint is included in the kinematics chain to match at best the robot to the patient. The AssistOn-SE [12] has through an innovative design one actuated linear DOF and one actuated rotational DOF for the compensation of SPR and one actuated linear DOF for the compensation of the SED. Moreover, a similar approach is adopted in the MEDARM [13] exoskeleton where two additional actuated joints are aligned with the sternoclavicular joint centre through one passive linear DOF.

Another approach to face this challenge consists in adding passive DOFs at the distal part or at the interface between the patient and the robot. The presence of these passive DOFs ensures that only desired efforts are transmitted to patient's joints regardless the robot structure or the alignment of the actuated robot joints on those of the patient. Such exoskeletons are called alignment-free exoskeletons because they aim to move the patient's joints without the necessity of aligning the robot joints with the patient's joints [14]. The ESA exoskeleton [15] and the ShoulderO [14] adopt such strategy for the shoulder complex. As a reminder, the self-aligning

This work was supported by the FRIA (Fonds pour la Recherche dans l'Industrie et l'Agriculture).

D. Galinski and B. Dehez are with the Center for Research in Mechatronics, Université catholique de Louvain, Louvain-la-Neuve, 1348, Belgium. e-mail: daniel.galinski, bruno.dehez@uclouvain.be.

exoskeletons have additional passive or actuated DOFs to align the robot joints on patient's joints. If these are passive, the drawback is that the robot structure must be carried by the distal part of the structure, i.e. the arm. If these are active, the drawback is the higher complexity of the device due to the necessity to control them through a zero force control-loop. As the structure of alignment-free exoskeletons must be carried by the proximal part, the alignment-free strategy is probably the most effective and the most compact approach for avoiding misalignments in shoulder rehabilitation exoskeletons.

Among these alignment-free exoskeletons, ShouldeRO has interesting characteristics such as ergonomics and compactness thanks to its 6-DOF poly-articulated mechanical structure which is actuated by two electrical jacks via a Bowden cable transmission. However, ShouldeRO has also several weaknesses. Firstly, the large friction and the relatively low stiffness of the Bowden cable transmission decreases the controllability and the bandwidth of the system. Secondly, the high complexity of the mechanical structure involves low reliability in practical use.

Based on these observations, an exoskeleton inspired from ShouldeRO was conceived. Its structure is constituted of two joints actuated through a direct-drive transmission to simplify the transmission and is linked to the patient through three passive joints to ensure the alignment-free behaviour. This paper details the optimal design of this new exoskeleton following a two step approach:

- 1) The first step involves an optimization process aiming at finding the best parameters characterizing the robot and positioning relative to the patient regarding two objective functions. These reflect the range of motion of the upper limb and the magnitude of parasitic efforts produced at the interface with the patient, which are the two most leading criteria in the performance evaluation of a rehabilitation robot.
- 2) The second step involves a comparison process aiming at selecting among the best solutions of the optimization regarding several criteria and comparing them to ShouldeRO. These criteria are quantitative but also qualitative criteria reflecting more practical aspects.

This paper is organized as follows. Section II presents the closed-loop model of the arm and the robot necessary both for the optimization. Section III details the objective functions and the constraints used for the optimization step. Section IV presents results of the optimization. Finally, Section V compares the best solutions generated with ShouldeRO to select the most promising solution for future prototyping.

II. CLOSED LOOP MODEL

A model of the closed loop kinematic chain formed by the arm and the exoskeleton is necessary to link the robot configuration to the arm orientation and to be able to evaluate criteria like workspace reachability used in the design process. This closed loop model is illustrated on Fig. 1 and detailed in the next subsections.

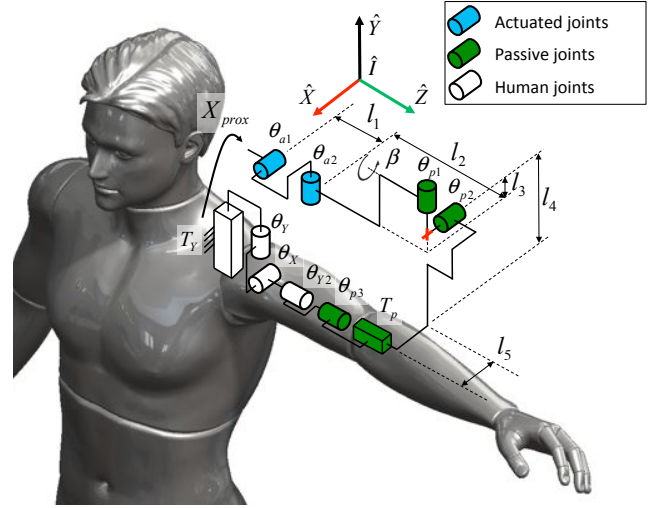


Fig. 1. Closed loop multibody model of the exoskeleton mounted on the arm at the initial position. The variables T_Y , θ_Y , θ_X , θ_{Y2} and θ_{p3} compose the arm model. The variables θ_{a1} and θ_{a2} are actuated and the variables θ_{p1} , θ_{p2} and T_p are passive joints of the exoskeleton.

A. Exoskeleton model

The exoskeleton considered in this study is directly inspired from ShouldeRO [14]. The alignment-free principle that consists in producing forces perpendicularly to the arm, is obtained in the same way thanks to the three mechanical passives joints θ_{p1} , θ_{p2} and T_p located on the robot distal part and the fourth passive DOF θ_{p3} , obtained by the free movement of the soft tissues around the humerus bone. It should be pointed out that the passive joints θ_{p1} and θ_{p2} are kinematically equivalent to a mechanical universal joint. These will be thus referred to as universal joint. The structure is the main difference with ShouldeRO. It is constituted of two actuated joints θ_{a1} and θ_{a2} perpendicular to each other. These permit to drive the two assisted joints θ_Y and θ_X of the shoulder complex.

The kinematics of the robot are defined, this robot can be completely characterized through six parameters shown in Fig. 1:

- l_1 is the distance between the two actuated joint axes θ_{a1} and θ_{a2} .
- l_2 is the distance between the axes of the second actuated joint θ_{a2} and the first passive joint θ_{p1} .
- β is the angle between the axes of the second actuated joint θ_{a2} and the first passive joint θ_{p1} .
- l_3 is the distance along the joint θ_{p1} between the axes of the second actuated joint θ_{a2} and the second passive joint θ_{p2} .
- l_4 is the distance between the axes of the second passive joint θ_{p2} and the centre of the limb.
- l_5 is the distance between the axes of the first passive joint θ_{p1} and the centre of the limb.

The position and the orientation of the first actuated joint θ_{a1} relative to the centre of the glenohumeral joint are characterized respectively through the parameters l_X , l_Y , l_Z and the parameters β_Y , β_Z . All of these parameters are components

of the vector \mathbf{X}_{prox} which is named as the proximal position of the robot.

B. Shoulder model

The International Society of Biomechanics (ISB) has described all the links in a human upper limb where each link can be represented by three angles [16]. Such a model is very complex and several papers have dealt with the simplification of the human arm model while keeping it able to describe precisely enough the upper limb kinematics [17]. The adopted model for the shoulder complex, as presented in the Fig. 1, is derived from the thorough simplifications presented in [18] and the model presented in [19]. These models consider two linear DOFs, along \hat{Y} and \hat{X} , in addition to three rotational DOFs, along \hat{X} , \hat{Z} and \hat{Y} , for the shoulder complex. Our model differs from these ones on two main points. Firstly, to ensure consistency with the recommendations of ISB, a Y-X-Y representation for the spherical joint of the shoulder complex has been preferred. Secondly, the scapular retraction-protraction, which corresponds to a linear DOF aligned with the \hat{X} axis, is neglected because its amplitude of motion is much lower than the scapular elevation-depression, which corresponds to the linear DOF aligned with the \hat{Y} axis. In a first approximation, this scapular elevation-depression is considered as linearly coupled to the elevation angle θ_X through the law:

$$T_Y = \begin{cases} 0 & \text{if } \theta_X \leq 0, \\ c \theta_X \text{ [m]} & \text{if } \theta_X > 0. \end{cases} \quad (1)$$

where the constant $c = 0.1$ [m/rad] was identified experimentally on a healthy subject.

III. OPTIMIZATION

The robot kinematics defined and parametrized, it can be used in an optimization process to find the best set of parameters regarding some objective functions and constraints. These are defined in the next two sections.

A. Objective functions

1) *Range-of-Motion*: The first objective function is directly related to the Range-of-Motion (ROM) of the shoulder along its two DOFs θ_X and θ_Y . Starting from the reference position of the arm presented in Fig. 1, the ideal ROM of the joints θ_X and θ_Y is assumed to be respectively from -90° (adduction) to $+60^\circ$ (abduction) and from -20° (arm backward) to $+90^\circ$ (arm forward). On this basis, the objective function is evaluated by discretizing the working space in 94 points uniformly distributed as shown in Fig. 3 (a) where crosses indicate the hand center positions. Each position is characterized by a weight proportional to its importance, 3 if the position is located at the most central points of the workspace (high importance) and 1 if the position is located at the most extreme points of the workspace (low importance). In each position, inverse kinematics is performed in order to find the position of the robot joints closing the loop with the arm. If this inverse kinematics converges, a score of 1 is attributed for

this position, 0 otherwise. The function F_1 is finally obtained from:

$$F_1 = - \frac{\mathbf{F}^T \mathbf{W}}{\sum_i \mathbf{W}_i} \quad (2)$$

where each element of the vector \mathbf{F} is the convergence score of the corresponding position and each element of the vector \mathbf{W} is the weight of the corresponding position.

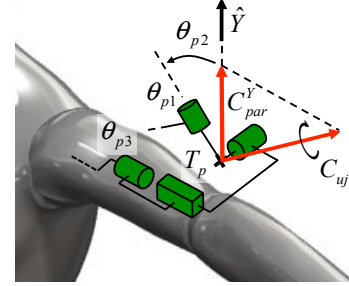


Fig. 2. Under specific conditions, a parasitic torque C_{par}^Y may appear due to the large amplitude of the second passive joint θ_{p2} .

2) *Parasitic efforts*: As explained in Section II-A, additional passive DOFs are introduced at the distal end of the robot in order to ensure the alignment-free principle of the robot. However, this behaviour is not always exactly met. Indeed, when the joint θ_{p2} is not in its initial position (as shown in Fig. 2), a part of the torque C_{uj} transmitted by the universal joint is applied on the limb. This component C_{par}^Y results from the projection of the torque C_{uj} on the axis \hat{Y} consequently to the effect of the passive DOF θ_{p3} .

The second objective function F_2 aims thus to be representative of this undesired phenomenon. Practically, for each of the 94 positions in the workspace when the inverse kinematics calculation has been made, inverse dynamics is performed on the model. During this inverse dynamics calculation, the robot remains motionless and a torque of 50 [Nm] is applied on the patient's joints θ_X and θ_Y to evaluate the induced parasitic torque C_{par}^Y . In order to cover all torque directions for each position, this calculation is made for eight different torque directions as shown in Fig. 3 (b). The function F_2 is finally calculated by applying the weight vector on the positions in a similar way to (2):

$$F_2 = - \frac{\mathbf{G}^T \mathbf{W}}{\sum_i \mathbf{W}_i} \quad (3)$$

where the global parasitic efforts vector \mathbf{G} of all positions is calculated by the following algorithm:

```

for all position  $j$  do
  calculate  $\mathbf{E}$  using (4).
  if  $\text{mean}(\mathbf{E}) \geq 50$  then
     $\mathbf{F}_j = 0$ 
     $\text{mean}(\mathbf{E}) = 50$ 
  end if
   $\mathbf{G}_j = \text{mean}(\mathbf{E})$ 
end for

```

TABLE I
INTERVALS OF PARAMETERS VARIATION FOR THE OPTIMIZATION

| | | |
|-------------|------------------------------------|-------------|
| l_X [cm] | l_Y [cm] | l_Z [cm] |
| [-14; 0] | [0; 13] | [-10; 0] |
| β_Y | β_Z | β |
| [-10°; 10°] | [0°; 90°] | [-90°; 90°] |
| l_1 [cm] | l_2 [cm] | l_3 [cm] |
| [0; 15] | [0; $l_{\text{arm}} - l_1 + l_Y$] | [-5; 5] |

where the vector \mathbf{E} is computed for every position on the basis of the parasitic forces calculated for the eight directions:

$$\mathbf{E} = (C_{\text{par}_1}^Y \quad \dots \quad C_{\text{par}_i}^Y \quad \dots \quad C_{\text{par}_8}^Y) \quad (4)$$

In this algorithm, if the parasitic efforts are high for a position, it means that the configuration is near a singularity. In this case, the first objective function F_1 is affected and the average of parasitic efforts is saturated to limit its effect on the second objective function F_2 .

B. Variables and constraints

The optimization variables are the parameters characterizing the robot geometry and its proximal positioning presented previously in the Section II-A. Their intervals of variation are shown in Tab. I excepting the parameters l_4 and l_5 defining the position of the universal joint relative to the limb centre for which two different cases are considered later. In addition, a constraint is imposed on the variable l_2 in order to ensure the position of the universal joint does not exceed the elbow when the shoulder is at its initial position (like shown in Fig. 1). This requirement can be formulated by:

$$l_1 + l_2 \leq l_{\text{arm}} + l_Y \quad (5)$$

where the arm length is $l_{\text{arm}} = 25$ [cm].

1) *Case 1 - Free universal joint*: The centre of the universal joint can be located inside the arm and the intervals of variation of the variables l_4 and l_5 are: $l_4 \in [-5; 5]$ and $l_5 \in [0; 10]$.

2) *Case 2 - Outer universal joint*: The universal joint must be located outside the arm. This possibility is considered because it is easier to materialize the universal joint when outside the arm. For this specific case, two other variables r and γ are used in the optimization algorithm. These latter are linked to the parameters by: $l_4 = r \sin(\gamma)$ [cm] and $l_5 = r \cos(\gamma)$ [cm]. To ensure the position of the universal joint outside the arm, the intervals of the variation of the variables r and γ are: $r \in [7; 15]$ [cm] and $\gamma \in [-45^\circ; 45^\circ]$.

C. Optimization algorithm

A genetic algorithm was selected as optimization algorithm for two reasons. Firstly, the presented optimization aims to be multi-objective. Secondly, it is impossible to extract any gradient from the evaluation of each solution due to the numerous non-linearities in the calculation of F_1 and F_2 .

A multiobjective genetic algorithm NSGA-II [20] implemented under Matlab© was used in this study. The initial population was created randomly and the algorithm was executed

on a population of 40 individuals for the two cases. The evolution of objective functions through iterations was observed periodically in order to detect the optimization convergence, i.e. when the values of objective functions of each individual do not change during several iterations. It was observed that 1000 iterations were enough to converge.

D. Evaluation

In practice, the evaluation of each solution follows the scheme shown in Fig. 3. The vector \mathbf{X} characterizing a solution is provided by the optimization algorithm. Each value of this vector is between 0 and 1 and is converted to model parameters \mathbf{X}_{prox} , β and \mathbf{l}_i by conversion laws which integrate constraints on the variables. Once converted, these parameters are integrated in the closed-loop model of the robot and the arm.

The model is automatically evaluated by Robotran™ which is a symbolic software for modelling and analyzing multibody systems [21]. An inverse kinematics simulation is first done for each discrete position of the shoulder complex. Next, the inverse dynamics simulation is executed by applying torques in eight directions for each position as previously explained. When these simulations are finished, the two objective functions are calculated in post-process and the results are returned to the optimization algorithm.

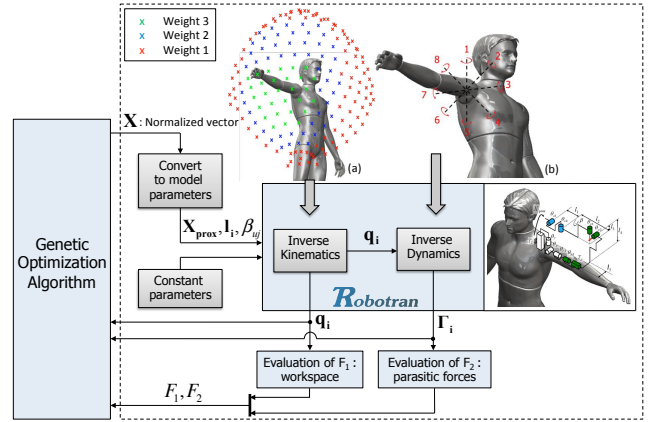


Fig. 3. Evaluation scheme of each solution.

IV. RESULTS

A. Case 1: Free universal joint

The Fig. 4 presents the Pareto front of the solutions resulting from the optimization with a free universal joint positioning. This front is not very marked since the best possible value for the objective function F_1 , i.e. -1 , is reached by almost all solutions. As a consequence, the function F_1 is not discriminative on the choice of individuals.

The analysis of the results leads to three main observations that apply to all solutions. Firstly, the universal joint is located at the centre of the limb since the distances l_4 and l_5 tends towards zero. Secondly, the distance l_1 between the two actuated joints θ_{a1} and θ_{a2} is small or close to zero, which is equivalent to an actuated spherical joint. Finally, all of the proximal positions of the robots are far from the center of the

shoulder complex and the variables l_X and l_Z tends towards -10 [cm]. This is due to the scapular elevation-depression of the shoulder taken into account in the model. This can be confirmed through the optimization process if the elevation parameter c in (1) is set to zero. In this case, the proximal position of all solutions is aligned with the glenohumeral joint and the passive DOFs become therefore useless. This a very interesting observation since it confirms that classical exoskeletons, i.e. exoskeletons requiring a perfect alignment of the robot joints on the patient's joints, should be the most appropriate solution in this specific but unrealistic case.

The unique differences between the solutions are the proximal orientation β_Y and β_Z , the universal joint orientation β , the distance the two actuated joints l_1 and the proximal elevation of the robot l_Y . The two most promising candidates, named as Solution 1 and Solution 2 in Fig. 4, are thus selected for further discussion since they differ significantly on these parameters, especially on the parameters l_1 , β and β_Z .

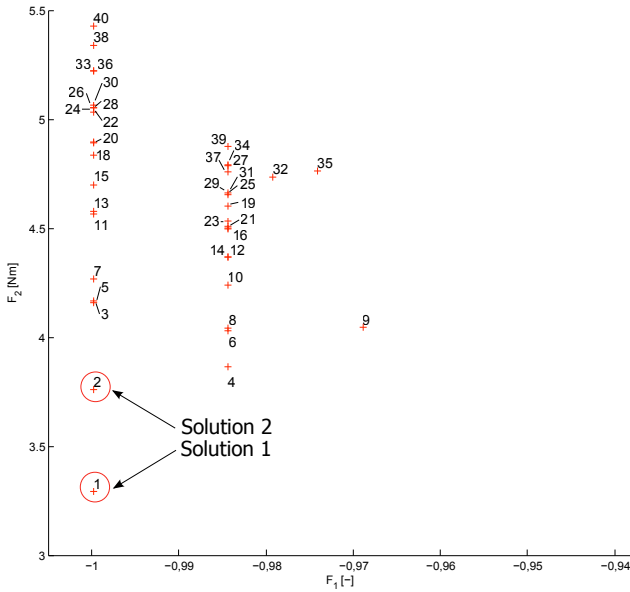


Fig. 4. Solutions space with a free positioning of the universal joint.

B. Case 2: Outer universal joint

The Fig. 5 presents the Pareto front of the solutions resulting from the optimization with a constrained positioning of the universal joint. It can be observed that the solutions are more dispersed in the objective function space than in the previous case.

Three main observations can be also made by analyzing the results. Firstly, the distance l_1 between the two motors is generally quite large. Secondly, the distance l_2 between the motor and the universal joint tends to its maximum length $l_{arm} - l_1 + l_Y$. Finally, there is one family of solutions where the proximal position of the robot is aligned with the glenohumeral centre. This observation is contrasting with the observations made on the previous case but their number is small and they are not the most effective. The others have their proximal position located behind the shoulder and far

from it. The most promising individual, named as Solution 3 in Fig. 5, is selected for further discussion.

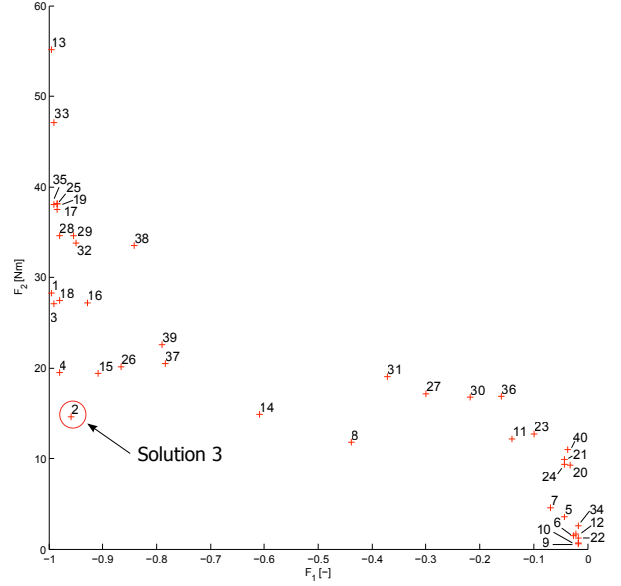


Fig. 5. Solutions space with an outer universal joint.

V. COMPARISON

The parameters and the values of the two objective functions that characterize the three selected solutions are presented in the first part of the Tab. II. These solutions are compared to ShouldRO considered for this study as the reference solution.

The determination of the best solution on the basis of two objective functions is not enough since it does not take into account the practical aspects linked to the materialization of the robot and to the necessity of avoiding collisions between the patient and the robot, for example. For that purpose, we introduced the following additional criteria:

- **Passive joints ROM:** the amplitude of motion of all passive joints, i.e. θ_{p1} , θ_{p2} , θ_{p3} and T_p should be minimized in order to simplify the robot and to make it as lightweight as possible or to limit the skin solicitation. From the results presented in Tab. II, it can be observed that all the solutions are almost equivalent except for the translational joint. For the latter, the solutions 1 and 2 are the best and the solution 3 the worst.
- **Manipulability:** the manipulability of the shoulder through the robot has to be maximized in order to guarantee the best controllability of the shoulder joints. According to [22], the manipulability M is given by $M = \det(\mathbf{J})$, where \mathbf{J} is in our case the Jacobian matrix linking the speeds of the actuated joints $\dot{\theta}_{a1}$ and $\dot{\theta}_{a2}$ to those of the shoulder joints $\dot{\theta}_Y$ and $\dot{\theta}_X$:

$$\begin{pmatrix} \dot{\theta}_Y \\ \dot{\theta}_X \end{pmatrix} = \mathbf{J} \begin{pmatrix} \dot{\theta}_{a1} \\ \dot{\theta}_{a2} \end{pmatrix} \quad (6)$$

This Jacobian matrix is dependent on the robot dimensions and positioning, but also on the shoulder joints position. It must therefore be computed for each solution

and for the 94 positions of the arm in the workspace through an inverse kinematics simulation. On this criteria, the solution 1 and 2 are equivalent and outperform the two others.

- Sensitivity: the sensitivity of the objective functions to the positioning of the robot relative to the patient must be minimized since this positioning will be difficult to control accurately in practice. This sensitivity was evaluated for each solution by perturbing the proximal positioning and orientation of the robot within a range of ± 1 [cm] and $\pm 5^\circ$ respectively and by computing the relative variations of the objective functions. A statistic analysis of the result for each solution shows that the three solutions 1, 2 and 3 are not very sensitive to perturbations in contrast to ShouldeRO.

In addition to these additional criteria, we also sketched a first embodiment of each solution taking into account the necessity of avoiding collisions between the robot and the patient in the entire workspace. On the basis of this embodiment, it seems interesting to evaluate also the solutions according to following qualitative aspects:

- Rigidity: The rigidity of the robot must be as high as possible to control at best the position of the arm whatever the interaction forces between the patient and the robot. This criterion can be linked to the shape and size of the mechanical parts constituting the robot but also to the transmission between the actuators and the actuated joints or to the way to materialize the passive joints. From this point of view, the materialization of a universal joint whose center is located outside of the arm, as for solution 3 and ShouldeRO, is simpler and more rigid than a universal joint whose centre is inside the limb, as for solutions 1 and 2. Moreover, the Bowden cable transmission used in ShouldeRO is much less rigid than the direct-drive used in the three new solutions.
- Complexity: The overall complexity of the robot is also a key factor because it directly affects the manufacturing costs and indirectly affects the global robot reliability. On this specific point, ShouldeRO is certainly the most complex due to the high number of DOFs of its mechanical structure and to its transmission. On the other hand, the solution 3 is the least complex because the materialization of the universal joint is simpler when its centre is located outside the arm.
- Ambidexterity: The ease with which a robot can be reconfigured to switch from a left to a right arm configuration is also an interesting criterion to take into account in the choice of the best solution. From this point of view, the solution 1 is judged very complex due to the geometrical configuration of the motors and the ShouldeRO is judged complex because the patient has to turn and to be located behind the robot to switch the arm. The ambidexterity of solution 2 and 3 gets a positive evaluation because just some parts of the robots has to be turned to switch the arm.

Based on these quantitative and qualitative criteria, it seems clear that the solution 2 is the best in terms of performance and

ergonomics even if the ROM of the universal joint is slightly larger than the universal joint of ShouldeRO.

VI. CONCLUSION

In this study, an optimal design aiming to find the characteristic dimensions and the proximal positioning of a rehabilitation robot minimizing two objective functions was presented. In a general case of robot design optimization, the same method may be applied with different objective functions for most meaningful criteria in the design or with different additional criteria helping to compare objectively all solutions resulting from the optimization. In this specific case, the method was applied on a alignment-free exoskeleton and the objective functions reflect the range of motion of the the shoulder and the ability to produce minimal parasitic efforts at the interface between the patient and the robot, which are judged as the most representative performance of a rehabilitation robot. The resulting solutions were then evaluated through additional criteria of less importance in post-process, to do not overburden the optimization process. These criteria are secondary in terms of performance but meaningful in terms of the materialization or the ergonomics of the robot.

This optimal design approach has led to a solution outperforming existing designs of alignment-free exoskeleton on several aspects as small transmission of parasitic efforts to patient, complete reachability of the shoulder ROM, low sensitivity to robot positioning, high manipulability in the entire workspace and several advantages linked to the materialization. Even if the ROM of the universal joint is bigger than in ShouldeRO, the retained solution is much lower complex and will be thus designed in detail in order to become the successor of ShouldeRO.

ACKNOWLEDGEMENTS

The authors would like to thank Mrs B. Herbin and D. Meert for their initial contribution in the algorithms developed for this study and the Robotran's team for their continuous advice for the development of evaluation algorithms. The authors would like also to thank the Belgian FNRS-FRIA, the Region Wallone and the first spin-off Axinesis project for their support in this work.

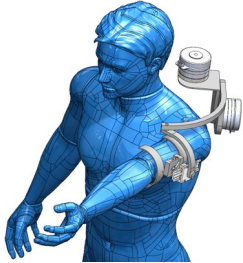
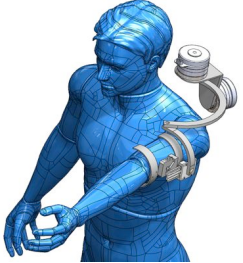
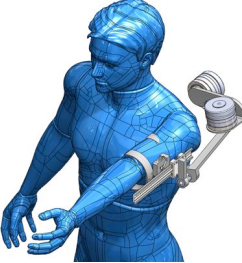

REFERENCES

- [1] Y. Bejot, I. Benatru, O. Rouaud, A. Fromont, J. P. Besancenot, T. Moreau, and M. Giroud, "Epidemiology of stroke in europe: Geographic and environmental differences," *Journal of the Neurological Sciences*, vol. 262, no. 12, pp. 85 – 88, 2007.
- [2] T. Truelsén, B. Piechowski-Jóźwiak, R. Bonita, C. Mathers, J. Bogousslavsky, and G. Boysen, "Stroke incidence and prevalence in europe: a review of available data," *European journal of neurology*, vol. 13, no. 6, pp. 581–598, 2006.
- [3] G. Prange, M. Jannink, C. Groothuis-Oudshoorn, H. Hermens, M. IJzerman *et al.*, "Systematic review of the effect of robot-aided therapy on recovery of the hemiparetic arm after stroke," *Journal of rehabilitation research and development*, vol. 43, no. 2, p. 171, 2006.
- [4] M. Van der Loos, "Robot-assisted movement training compared with conventional therapy techniques for the rehabilitation of upper-limb motor function after stroke," *Arch Phys Med Rehabil*, vol. 83, 2002.
- [5] G. Kwakkel, B. Kollen, and H. Krebs, "Effects of robot-assisted therapy on upper limb recovery after stroke: a systematic review," *Neurorehabilitation and neural repair*, vol. 22, no. 2, pp. 111–121, 2008.

TABLE II

SYNTHESIS OF SELECTED SOLUTIONS AND COMPARISON TO SHOULDERO [14].

* AN OPTIMIZATION OF THE PROXIMAL POSITION OF SHOULDERO WAS MADE IN ORDER TO FIND THE MOST FAVOURABLE POSITION OF SHOULDERO.
 † THE VALUES OF THE VARIABLES ARE SHOWN IN THE FORM OF MEAN \pm STANDARD DEVIATION.

| | Solution 1 | | Solution 2 | | Solution 3 | | ShoulderO [14] | |
|--------------------------------|--|----|--|----|---|----|--|---|
| Variables | | | | | | | | |
| l_1 [cm] | (2.2; 25.1; -2.0; 0; 0) | | (0; 28.4; -3.9; 0; 0) | | (13.7; 26.2; -5.1; 5.0; 0) | | N/A | |
| β [-] | -80° | | 0° | | 10° | | 0° | |
| X_{prox} [(cm)] ([-]) | (-10; 3.5; -10) (-10° ; 83°) | | (-10; 1.5; -10) (-10° ; 10°) | | (-12; 0; -10) (7° ; 0°) | | (-14; 10; 0) (0; 0)* | |
| Objective functions | | | | | | | | |
| F_1 [-] | -1 | + | -1 | + | -0.96 | 0 | -0.95 | 0 |
| F_2 [Nm] | 3.29 | ++ | 3.76 | ++ | 14.58 | + | 42.63 | 0 |
| ROM | | | | | | | | |
| θ_{p1} [-]† | $4.0^\circ \pm 17.8^\circ$ | - | $-0.6^\circ \pm 16.0^\circ$ | - | $-9.2^\circ \pm 20.1^\circ$ | -- | $7.4^\circ \pm 6.9^\circ$ | 0 |
| θ_{p2} [-]† | $6.9^\circ \pm 17.2^\circ$ | - | $-9.2^\circ \pm 13.8^\circ$ | - | $14.9^\circ \pm 27.5^\circ$ | -- | $13.2^\circ \pm 5.2^\circ$ | 0 |
| T_p [cm]† | 2.3 ± 1.2 | + | 2.2 ± 1.2 | + | 24.2 ± 19.1 | - | 5.0 ± 3.2 | 0 |
| θ_{p3} [-]† | $43.0^\circ \pm 14.3^\circ$ | - | $113.4^\circ \pm 20.0^\circ$ | - | $94.5^\circ \pm 26.4^\circ$ | - | $25.8^\circ \pm 10.3^\circ$ | 0 |
| Manipulability [-]† | 0.88 ± 0.14 | + | 0.88 ± 0.15 | + | 0.68 ± 0.31 | 0 | 0.64 ± 0.26 | 0 |
| Sensitivity | medium | + | low | + | medium | + | high | 0 |
| Materialization | | | | | | | | |
| |  | |  | |  | |  | |
| Rigidity of distal part | medium | + | medium | + | high | ++ | low | 0 |
| Parts complexity | medium | + | medium | + | low | ++ | high | 0 |
| Ambidexterity | very complex | - | easy | + | easy | + | complex | 0 |
| SYNTHESIS | 4 '++' | | 6 '++' | | 1 '++' | | reference | |

- [6] M. Gilliaux, T. Lejeune, C. Detrembleur, J. Sapin, B. Dehez, and G. Stoquart, "A robotic device as a sensitive quantitative tool to assess upper limb impairments in stroke patients: A preliminary prospective cohort study," *Journal of Rehabilitation Medicine*, vol. 44, no. 3, pp. 210–217, 2012.
- [7] T. Nef, M. Guidali, and R. Riener, "Armin iii-arm therapy exoskeleton with an ergonomic shoulder actuation," *Applied Bionics and Biomechanics*, vol. 6, no. 2, pp. 127–142, 2009.
- [8] R. Sanchez Jr, E. Wolbrecht, R. Smith, J. Liu, S. Rao, S. Cramer, T. Rahman, J. Bobrow, and D. Reinkensmeyer, "A pneumatic robot for re-training arm movement after stroke: Rationale and mechanical design," in *Rehabilitation Robotics, 2005. ICORR 2005. 9th International Conference on*. IEEE, 2005, pp. 500–504.
- [9] A. Stienen, E. Hekman, H. ter Braak, A. Aalsma, F. van der Helm, and H. van der Kooij, "Design of a rotational hydroelastic actuator for a powered exoskeleton for upper limb rehabilitation," *Biomedical Engineering, IEEE Transactions on*, vol. 57, no. 3, pp. 728–735, 2010.
- [10] H. Park, Y. Ren, and L. Zhang, "Intelliarm: An exoskeleton for diagnosis and treatment of patients with neurological impairments," in *Biomedical Robotics and Biomechanics, 2008. BioRob 2008. 2nd IEEE RAS & EMBS International Conference on*. IEEE, 2008, pp. 109–114.
- [11] D. Koo, P. Chang, M. Sohn, and J. Shin, "Shoulder mechanism design of an exoskeleton robot for stroke patient rehabilitation," in *Rehabilitation Robotics (ICORR), 2011 IEEE International Conference on*. IEEE, 2011, pp. 1–6.
- [12] M. Ergin and V. Patoglu, "Assiston-se: A self-aligning shoulder-elbow exoskeleton," in *Robotics and Automation (ICRA), 2012 IEEE International Conference on*. IEEE, 2012, pp. 2479–2485.
- [13] S. Ball, I. Brown, and S. Scott, "Medarm: a rehabilitation robot with 5dof at the shoulder complex," in *Advanced intelligent mechatronics, 2007 IEEE/ASME international conference on*. IEEE, 2007, pp. 1–6.
- [14] B. Dehez and J. Sapin, "Shouldero, an alignment-free two-dof rehabilitation robot for the shoulder complex," in *Rehabilitation Robotics (ICORR), 2011 IEEE International Conference on*. IEEE, 2011, pp. 1–8.
- [15] A. Schiele and G. Visentin, "The esa human arm exoskeleton for space robotics telepresence," in *7th International Symposium on Artificial Intelligence, Robotics and Automation in Space*, 2003, pp. 19–23.
- [16] G. Wu, F. Van der Helm, H. Veeger, M. Makhsoos, P. Van Roy, C. Anglin, J. Nagels, A. Karduna, and K. McQuade, "ISB recommendation on definitions of joint coordinate systems of various joints for the reporting of human joint motion—Part II: shoulder, elbow, wrist and hand," *Journal of biomechanics*, vol. 38, no. 5, pp. 981–992, 2005.
- [17] D. Galinski and B. Dehez, "Evaluation of initialization procedures for estimating upper limb kinematics with marg sensors," in *IEEE International Conference on Biomedical Robotics and Biomechanics*, 2012.
- [18] N. Klopčar and J. Lenarčič, "Kinematic model for determination of human arm reachable workspace," *Meccanica*, vol. 40, no. 2, pp. 203–219, 2005.
- [19] D. Romilly, C. Anglin, R. Gosine, C. Hershler, and S. Raschke, "A functional task analysis and motion simulation for the development of a powered upper-limb orthosis," *Rehabilitation Engineering, IEEE Transactions on*, vol. 2, no. 3, pp. 119–129, 1994.
- [20] K. Deb, A. Pratap, S. Agarwal, and T. Meyarivan, "A fast and elitist multiobjective genetic algorithm: Nsga-ii," *IEEE Transactions On Evolutionary Computation*, vol. 6, no. 2, 2002.
- [21] J. Samin and P. Fiset, *Symbolic modeling of multibody systems*. Springer Netherlands, 2003.
- [22] M. Spong, S. Hutchinson, and M. Vidyasagar, *Robot modeling and control*. John Wiley & Sons Hoboken, 2006.